Investigation of the deposition and thermal behavior of striped phases of unsymmetric disulfide self-assembled Monolayers on Au(111): The case of 11-hydroxyundecyl decyl disulfide

Erol Albayrak,[a] *Semistan Karabuga,*[b] *Gianangelo Bracco,*[c] *M. Fatih Danışman*[*,d]

[a] Department of Materials and Metallurgical Engineering, Ahi Evran University, Kırşehir 40000, Turkey

[b] Department of Chemistry, Kahramanmaraş Sütçü İmam University, Kahramanmaraş 46030, Turkey

[c] CNR-IMEM and Department of Physics, University of Genoa, via Dodecaneso 33, Genoa 16146, Italy

[d] Department of Chemistry, Middle East Technical University, Ankara 06800, Turkey

KEYWORDS: 11-(decyldisulfanyl)undecan-1-ol, thiol SAMs, low energy atom scattering, supersonic molecular beam deposition

ABSTRACT: Self-assembled monolayers (SAMs) of unsymmetric disulfides on Au(111) are used to form mixed SAMs that can be utilized in many applications. Here, we have studied 11-hydroxyundecyl decyl disulfide (CH_3-$(CH_2)_9$-S-S-$(CH_2)_{11}$-OH, HDD) SAMs produced by supersonic molecular beam deposition (SMBD) and characterized by He diffraction. The film growth was monitored at different temperatures up to a coverage which corresponds to a full lying down phase and the diffraction analysis shows that below 250 K the phase is different from the phase measured above 300 K. During the annealing of the film, two phase transitions were observed, at 250 K and 350 K. The overall data suggest that the former is related to an irreversible phase separation of HDD above 250 K to decanethiolate (-S-$(CH_2)_9$-CH_3, DTT) and hydroxyundecylthiolate (-S-$(CH_2)_{11}$-OH, MUDT), while the latter to a reversible melting of the film. Above 450 K the specular intensity shows an increase related to film desorption and different chemisorbed states were observed with energies in the same range as observed for decanethiol (H-S-$(CH_2)_9$-CH_3, DT) and mercaptoundecanol (H-S-$(CH_2)_{11}$-OH, MUD) SAMs.

INTRODUCTION

Thiol self-assembled monolayers (SAMs) on Au(111) surfaces have a variety of applications ranging from molecular electronics to biocompatible/bioactive surfaces.[1-7] Their fundamental properties, like crystal structures, adsorption dynamics and mechanism are very important both from a pure scientific point of view and due to their implications on the performance of the applications. [1-7]

For realization of many different purposes, like obtaining a hydrophobic surface for instance, use of single component SAMs is sufficient, hence, properties and film formation dynamics/mechanism of such SAMs, which can be formed by using thiols (R-S-H) or symmetric disulfides (R-S-S-R), are well established.[2,4,8-15] The monolayer presents two different regimes depending on the density. At low density, i.e. low coverage, molecules were observed to form rectangular unit cells (p x √3), the so called striped phases, where the periodicity p, which depends on the film density and the length of the molecule, gives the stripe separation along the gold nearest neighbor azimuthal direction. [3,4,10,15-23] Upon increasing the coverage, the contribution of the interaction between alkyl chains becomes more important and allows the formation of a standing up configuration with the (√3 x √3)R30° structure.[4,20,24,25] For many other applications like controlled protein adsorption [5,6] or polymer growth on a surface [26], however, utilization of mixed SAMs, which are made up of two or more components, may be necessary. Such films are produced either by co-adsorbing different thiols (i.e. R-S-H and R'-S-H) in solution or by using unsymmetric disulfides (R-S-S-R'). In the former method SAM composition can be varied by controlling the

mole fractions of the precursor thiols in the growth solution. However, the mole fraction of the components in the SAM may deviate from their mole fractions in the growth solution and phase separation may take place in the SAM depending on the concentrations of the precursor thiols in the solution and their chemical/structural degree of difference.[27-36] The latter method, on the other hand, suffers from the low solubility of disulfides and controlled variation of composition is not possible due to 1:1 ratio of R and R' groups. Nevertheless large deviations from 1:1 ratio in the unsymmetric disulfide SAM were observed due to chemical/structural difference of R and R' groups.[37,38] One of the more studied issues regarding unsymmetric disulfide SAMs is whether a phase separation takes place or not, which has implications in preparation of patterned surfaces and which is a way of determining if S-S bond cleaves during adsorption. [39-43] In case of full coverage (high density) SAMs of CH_3-$(CH_2)_m$-S-S-$(CH_2)_n$-OH no phase separation was observed by several research groups. [40-42] On the other hand for m=17 and n=11 phase separation was observed at low coverage which was evidenced by the formation of two different corrugation periodicities consistent with the lengths of separated thiolates. [43]

In order to contribute to the understanding of the behavior of unsymmetric disulfides SAMs on Au(111) surface, which so far had been grown only from solution, we have studied SAMs of 11-hydroxyundecyl decyl disulfide (CH_3-$(CH_2)_9$-S-S-$(CH_2)_{11}$-OH, HDD) grown in vacuum by means of supersonic molecular beam deposition (SMBD) which enabled us to control film coverage very precisely. The separate thiols forming this disulfide, namely decanethiol [CH_3-$(CH_2)_9$-S-H, DT] and mercaptoundecanol [H-S-$(CH_2)_{11}$-OH, MUD], had been studied in the past in detail both by our group[15,44] and by other research groups[17,21,45,46] and their properties are well known. DT films, for instance, form lying down monolayers at low coverage with (11 $\times\sqrt{3}$) striped lattice structure where the distance between stripes is 11 times the Au(1 1 1) lattice constant (2.884 Å) and the

periodicity within the stripes is √ 3 times the Au(1 1 1) lattice constant. MUD films, however, were reported to form a (11.8×√3) striped phase [44] [(12×√3) in ref. 45]. In addition both films undergo a solid-liquid phase transition at around 350 K [15,46] and 400 K [44] respectively. Here, by using helium diffraction we were able to monitor HDD film growth in real time and follow the evolution of film structure as a function coverage and substrate temperature to gain further evidence on the occurrence of phase separation by comparing the results with those previously reported for MUD and DT.

EXPERIMENTAL

The experimental setup was extensively described before [47] and here we give only a brief description related to the present experiment. The helium diffraction apparatus is connected to secondary vacuum chamber which houses an SMBD source made of a Pyrex tube with a ≈100 μm diameter nozzle. A small Pyrex reservoir, filled with the organic material to be deposited, is inserted in the tube which can be heated by a coil heater to cause the sublimation of the organic material. The organic vapor and the helium carrier gas form a mixture which expands through the nozzle in the secondary vacuum chamber forming a seeded beam which passes through a skimmer before to impinge on the surface of the substrate at the center of the main chamber of the diffraction apparatus. Reasonable HDD flux values were achieved at source temperatures of 130°C - 145°C. By comparing the NMR spectra of the organic source material recorded before and after deposition experiments, it was confirmed that heating to 130°C - 145°C for deposition did not damage the HDD molecules. The impinging energy of the HDD was not measured; however by assuming ideal expansion conditions to obtain the terminal speed of the carrier gas and a thiol concentration of less than 1% in the beam, the maximum incident kinetic energy can be calculated to be in the range of 4.2 eV – 8.5 eV.[48] The disulfides present relatively flexible alkyl chains and during the

impact with the surface several atoms can be involved in the process reducing the effective energy per atom. The collision with the surface is therefore softer than expected by considering only the total kinetic energy, but in any case higher than the thermal energy and this may help to induce surface diffusion and in case S-S bond breaking.

The characterization of the deposited films were carried out by using a supersonic beam of helium (purity 99.9999%), produced in the supersonic source of the apparatus working at about 70 K. At this temperature, the wave vector is $k_i = 5.13$ Å^{-1}, which corresponds to a kinetic energy of 14 meV, with a velocity spread of 2%. Diffraction measurements were performed for a substrate temperature between 60 K and 80 K to reduce the effect of vibrations. Diffraction scans were acquired along different crystallographic directions on the surface to reconstruct the unit cell of the structures. For this purpose a bolometer detector, cooled with liquid helium, was rotated around the sample in the plane containing the incident helium beam and the surface normal, i.e. the scattering plane, as depicted in Figure 1. To optimize the detected intensity, the rectangular slit in front of bolometer has a narrow size in the scattering plane and a larger size in the perpendicular direction (along the rotation axis), hence our instrument has a good angular resolution in the scattering plane while the azimuthal resolution is relaxed as graphically shown in Figure 1. The angular data were converted to momentum space by using the equation $\Delta K_{//} = k_i(\sin \theta_f - \sin \theta_i)$ where $\Delta K_{//}$ is the parallel momentum transfer, and θ_i and θ_f are the incident angle and the detector angular position with respect to surface normal, respectively. The Au(111) surface with an orientation accuracy of <0.1° was purchased from Mateck GmbH. Before each experiment the surface was treated with several sputter-anneal cycles and the cleanness was confirmed by observation of the gold reconstruction diffraction peaks and a specular reflection intensity of no less than 25% of the incident beam.

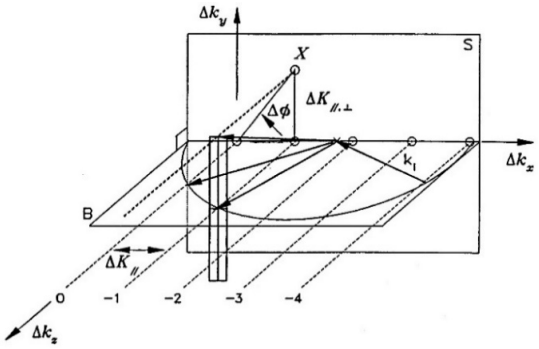

Figure 1. Detection scheme depicting the scattering geometry and the detector function.

The investigation of helium specular reflection (SR) as a function of the surface temperature allows the estimation of desorption energies. In fact increasing the temperature, the SR intensity decreases due to the increasing of the amplitude of thermal vibrations, i.e. the Debye-Waller effect. An organic film generally is softer therefore the SR intensity from the film is smaller than the intensity of the bare substrate at the same temperature. Moreover the film is generally less ordered than the substrate, and since He diffraction is also very sensitive to surface disordering, the scattered intensity from an organic film is further decreased by this disordering. When the organic film starts to desorb, uncovering the substrate surface, the intensity increases until the surface is clean and the SR intensity of the bare substrate is recovered. For a further temperature increase the SR intensity decreases with the trend of the clean substrate. The derivative of the SR intensity during the film desorption, corrected for Debye-Waller effect and detector sensitivity, plotted against the sample temperature yields a peak which is related to the conventional temperature programmed desorption peak. [8] The estimation of adsorption energies for the desorbing species is obtained by a Redhead analysis [49] of the peaks in the derivative of SR intensity. In this study crystal temperature was ramped with the same rate in all the measurements at 0.8-1.3 K/s. Above 400 K, the sensitivity of our detector starts to decrease due to absorbed radiation emanated by the sample and therefore we generally limit the analysis below this temperature. For the Redhead analysis, a

first-order desorption and a coverage independent desorption energy were assumed. Though these assumptions may be questioned the energies calculated this way can still be used for comparison with the energies reported before in the literature determined by using similar procedures/assumptions. In our sample holder made in copper, the substrate temperature is measured by a platinum thermometer which is near but not in direct contact with the gold crystal. We estimated that the measurements are affected by an error bar of ± 5 K and the estimated errors on calculated desorption energies also include this temperature contribution.

HDD was synthesized as follows by following the procedure proposed by Flores et al. [42]: Decanethiol (3.5 mmol) was added to the solution of diethylazadicarboxylate (DEAD) (3.5 mmol) in 20 ml of diethyl ether at room temperature. The reaction mixture was stirred for 3 days. After evaporation of solvent at reduced pressure, the crude mixture was dissolved in 20 ml of dichloromethane (DCM). The mixture of reaction was added mercaptoundecanol (3.5 mmol) and refluxed for 2 days, monitored by TLC. After the reflux period the solvent was concentrated under vacuum and the crude product was purified by column chromatography by eluting with hexane and ethyl acetate (v/v, 6:1). Yield: 25%; mp 55-58ºC; ^{1}H NMR(400 MHz, $CDCl_3$, ppm) δ 3.64 (t, J = 6.6 Hz, 3H), 2.68 (t, J = 7.3 Hz, 6H), 1.67 (td, J = 14.9, 7.3 Hz, 4H), 1.60-1.52 (m, 2H), 1.44-1.19 (bm, 28H), 0.88 (t, J = 6.8 Hz, 3H)

RESULTS

In this section we present the He diffraction measurements performed on the organic film. In the first part we will consider the trend of SR intensity for the deposition of the film at different sample temperatures beyond the formation of a monolayer of lying down molecules. In the second part, the study of the low coverage region is reported and, in the third one, we will compare the diffraction patterns of monolayer films grown at different substrate temperatures. In the last part

we will discuss the effect of thermal treatments performed on monolayer films and their thermal stability.

I. Deposition of the film at different substrate temperatures

In Figure 2 the deposition curves for different substrate temperatures are shown. The SR intensity is normalized to the zero coverage value and this intensity is plotted vs. the film coverage. The curves show a general behavior with a SR intensity that decrease as film coverage increases. In fact, the clean and smooth metal surface is randomly covered by molecules which increase the surface roughness of the system therefore some of the intensity is scattered as a diffuse background. Moreover the film is softer than the metal and the low energy vibrations further reduce the elastically scattered intensity. As the first monolayer (ML) completes however the film acquires an ordering and a relatively smoother surface forms that results in a partial recovery of the SR intensity. In fact the coverage values in Figure 2 were deduced from the deposition times by assigning 1 ML coverage to the deposition times that correspond to these recovery maxima. Here we should also note that by ML we refer to full monolayer lying down striped phase but not the high density standing up monolayer phase. After completion of the ML, further adsorption, again, increases the surface roughness till it reaches a steady state resulting in a constant low SR intensity signal, very likely due to a three dimensional growth of multilayers. The shapes of the deposition curves however show a pronounced difference depending on the surface temperature. Below 265 K and above 300 K the SR intensity recovery is pronounced and the decay after the recovery is sharp (see the inset in Figure 2). At 265 K and 300 K the recovery is not pronounced and it only appears as a shoulder. Finally at 400 K the recovery becomes very broad and the decay after the recovery is much slower and limited when compared with the lower substrate temperatures.

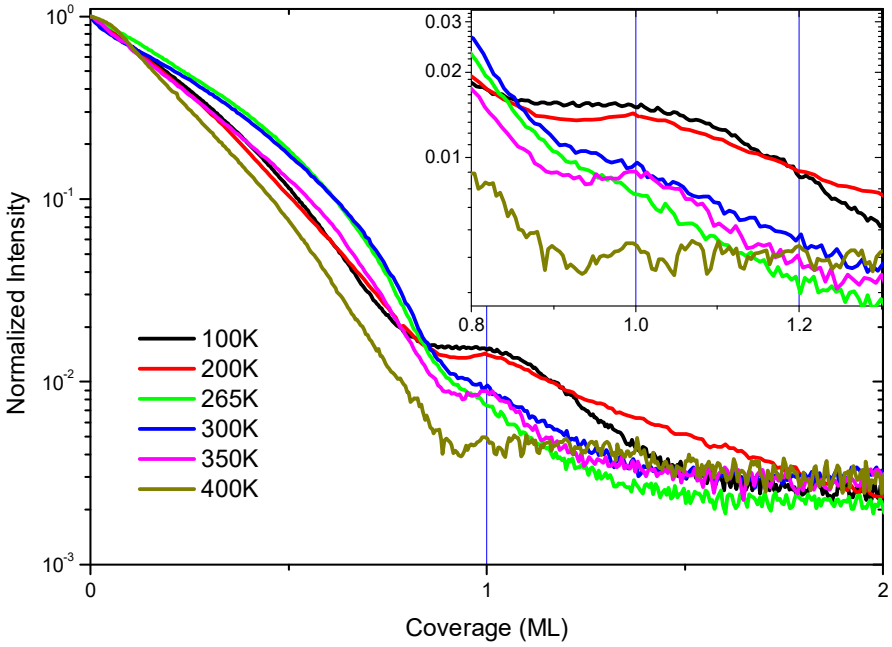

Figure 2. Deposition curves showing helium specular reflection intensity as a function of HDD coverage on Au(111) at different substrate temperatures. Inset shows a zoomed view of the region around 1 ML.

II. Diffraction pattern of as-deposited monolayer films

In the following discussion we will only focus on the lying down ML phases and discuss their structural and thermal properties in detail. In Figure 3 diffraction scans of representative ML films for each temperature range discussed above are shown. For recording these scans, deposition was stopped at ML coverage and the diffraction data were recorded at 60 K – 80 K substrate temperature. For films grown at high surface temperatures (300 K and 350 K) similar diffraction patterns were observed with clear $\sqrt{3}$ peaks at about 2.54 $Å^{-1}$ along the <11-2> direction and striped phase peaks along the <1-10> directions, consistent with previous observed striped phases. (The peaks around the specular peak along the <11-2> direction are off azimuth peaks associated with

nearby directions and are an outcome of the limited azimuthal resolution of our diffractometer.) This ML phase hereafter will be referred to as high temperature (HT) phase. Instead for film grown at 200 K, although the SR intensity is similar to the HT phase, the observed diffracted peak positions indicate the formation of a different film structure. Moreover this phase is less ordered with respect to the HT phase since the peak widths and the diffuse background are larger. This ML phase will be referred to as low temperature (LT) phase hereafter. The ML grown at 265K however seems to be a transition structure from the LT phase to the HT phase, since its diffraction pattern presents some features similar to that of HT and LT phases, but, respect to the HT phase, with much broader and lower intensity diffraction peaks. In addition this film has the lowest specular reflection intensity when compared with the other two films which implies that it has the highest roughness.

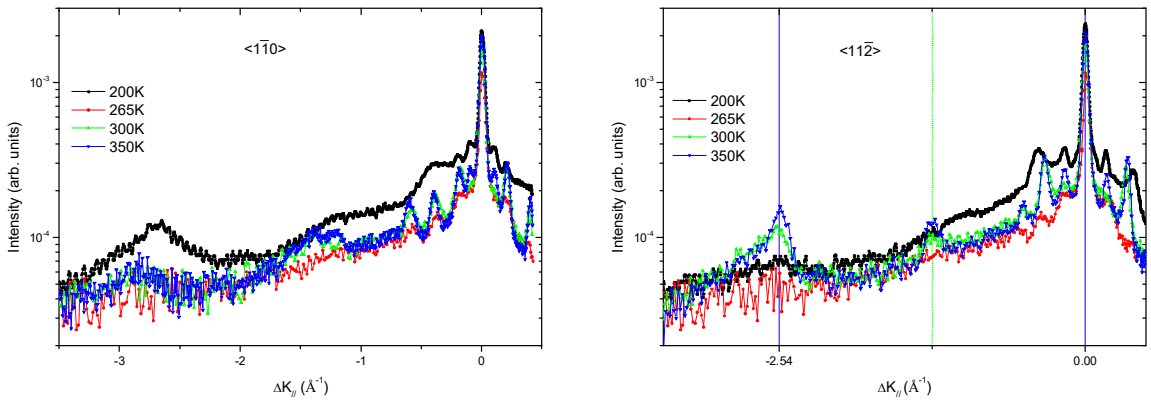

Figure 3. Diffraction scans measured along the main azimuthal directions of Au(111) for ML films grown at different substrate temperatures.

III. Thermal treatment of lying down monolayers

To study the thermal stability of LT and HL phases, we annealed them at/to different temperatures while monitoring SR intensity and followed the evolution of film structure with annealing temperature.

In Figure 4, heating and cooling curves of ML films grown at 200, 265 and 300 K are shown. With increasing temperature SR intensity decreases due to increasing thermal motion of the surface atoms/molecules as a general trend for all the films. During heating of the ML grown at 200 K (LT phase), SR intensity decay rate increases at 250 K and then decreases suddenly at 275 K. Stopping the annealing at 350 K and cooling the sample, this change in the decay rate is not reversible and is not present in the cooling curve. For the MLs grown at 265 K, the SR intensity during annealing to 350 K has a monotonic decrease but its value is less than the value of the 200 K film, instead the cooling curve is equal to the previous one. This means that the *as deposited* 200 K film is flatter and very likely more order than the equivalent 265 K film, after the annealing to 350 K the two films present the same order. For the ML grown at 300 K the heating curve has a monotonic trend and its intensity is similar to that of the cooling curves of both previous films. After annealing to 375 K, the cooling curve is slightly higher than the other cooling curves but with a similar slope. This means that the *as deposited* 300 K phase has an order similar to the previous *annealed* films and an annealing to higher temperature is beneficial to get a better order.

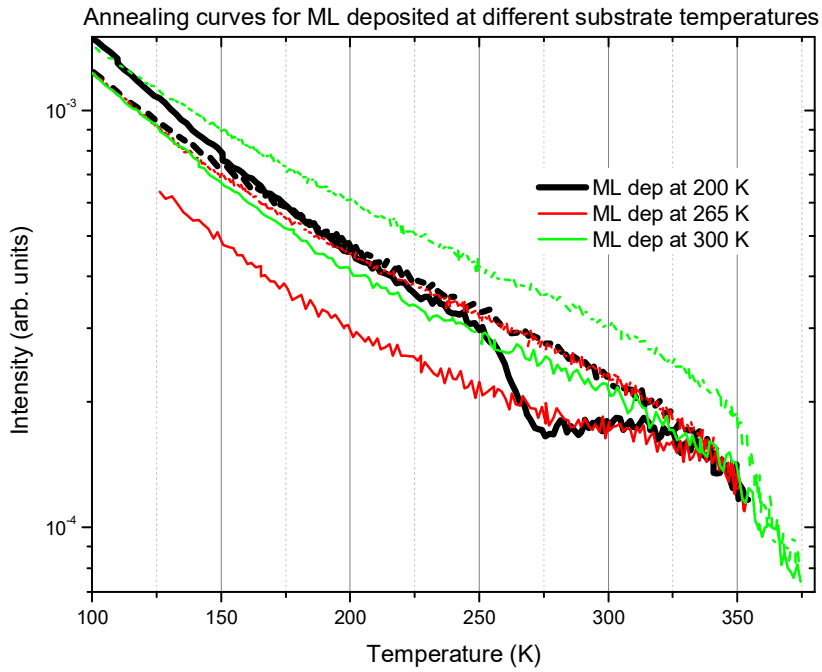

Figure 4. Heating (solid) and cooling (dashed) curves for ML films deposited at different substrate temperatures.

The comparison of the heating-cooling cycles shows that the LT phase undergoes an irreversible transition in the range 250-275 K which transform the LT into the HT phase. The comparison between the heating curve of the 200 K film and the cooling curve of the 300 K film shows that they have a similar SR intensity below 120 K, but the intensity decay is faster for the 200 K film. This points out that the 200 K film, i.e. the LT phase, presents a larger Debye Waller effect and in turn a larger mean square displacements with respect the HT phase, hence the LT phase is softer than the HT phase.

As shown in Figure 4, an annealing at temperatures higher than 350 K can improve the order of the film but a closer inspection of the curves shows faster intensity decay above 350 K. To gain insights on this decay we annealed ML films grown at 200 K to different maximum temperatures recording the heating and cooling curves. A summary of this investigation is shown in Figure 5a.

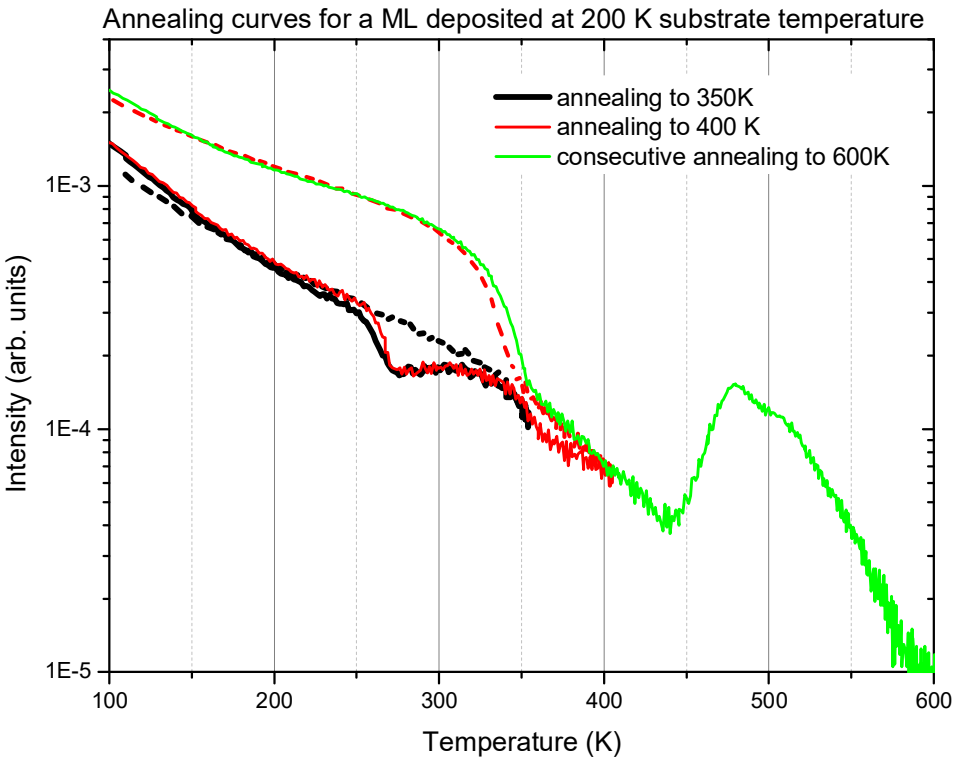
Annealing curves for a ML deposited at 200 K substrate temperature
annealing to 350K
annealing to 400 K
consecutive annealing to 600K
Intensity (arb. units)
1E-3
1E-4
1E-5
100
200
300
400
500
600
Temperature (K)

a)

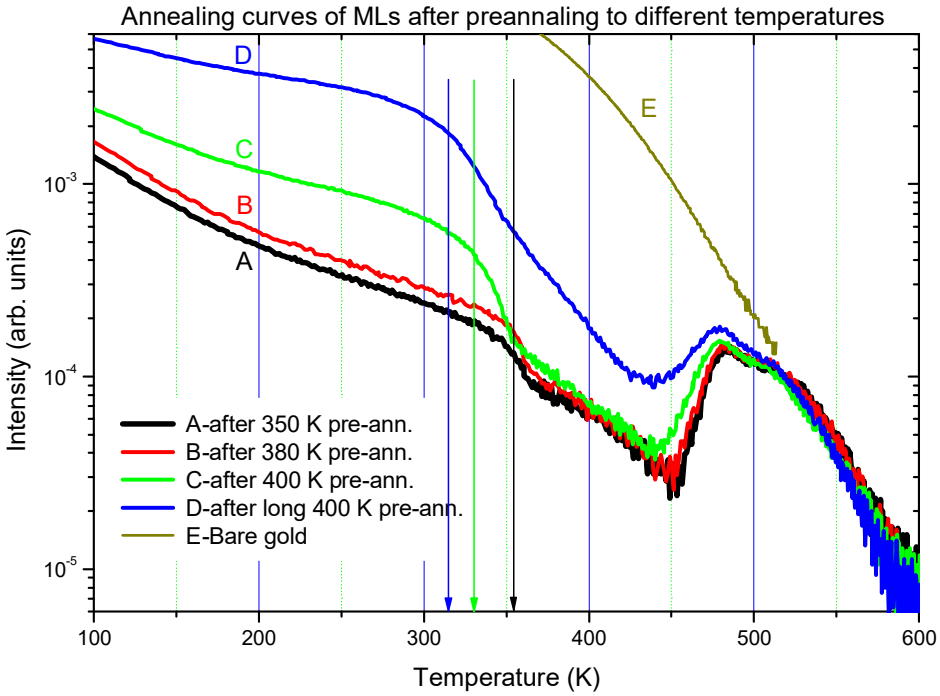
Annealing curves of MLs after preannaling to different temperatures
D
C
B
A
E
Intensity (arb. units)
10-3
10-4
10-5
A-after 350 K pre-ann.
B-after 380 K pre-ann.
C-after 400 K pre-ann.
D-after long 400 K pre-ann.
E-Bare gold
100
200
300
400
500
600
Temperature (K)

b)

Figure 5. a) Heating (solid) and cooling (dashed) curves for two different ML films deposited at 200 K substrate temperature, one annealed to 350 K, the other annealed to 400 K and then consecutively to 600 K. b) Heating curves recorded after pre-annealing MLs to different temperatures. The plots shown here are not corrected for the detector sensitivity and the Debye-Waller effect. The vertical arrows show the transition temperature for the curves A, C, and D.

In the first heating curve up to 350 K, the curve displays the irreversible transition below 300 K and around 350 K a suggestion of an increased decay rate, the cooling curve essentially overlaps with the heating curve (except in temperature interval of 250 K-320K where the irreversible low temperature phase transition took place while heating). Performing an annealing-cooling cycle to 400 K on another film deposited at 200 K, the cooling curve shows a substantial increase of the intensity starting at 350 K. Performing a consecutive annealing to 600 K on the same film, the heating curve follows the trend of the previous cooling curve up to 400 K. Apart a slight hysteresis, this clearly shows that the intensity decay is due to a reversible transition between 330 K and 350 K. At 430 K (the minimum of the intensity) the slope becomes positive with a maximum (desorption peak) at 480 K which is related to the desorption of the organic film. The maximum is followed by a shoulder at 510 K which is associated with another desorption from a different adsorption state.

To study the effects of annealing on the reversible phase transition, we pre-annealed different MLs first to temperatures between 350 and 400 K and then heated them to 600 K as shown in Figure 5.b. Up to 380 K pre-annealing no change occurs in the phase transition temperature interval (curves A and B), only the heating curve with the higher pre-annealing temperature (curve B) shows more intensity at temperatures below the transition, due to the reordering of the film, but

above 370 K the curves A and B overlap up to desorption peak. This indicates that, although the film annealed to higher temperature is more ordered at lower temperature, above the transition both films have similar structure.

Instead, the onset of the phase transition for the curve corresponding to a pre-annealing to 400 K (curve C) shifts to lower temperatures, as indicated by the arrows in the Figure 5.b. In addition, the intensity minimum shifts to a lower temperature along with the maximum of the desorption peak. Furthermore, pre-treating the sample with a longer annealing at 400 K for 6 minutes (curve D), the SR intensity increases significantly while the onset of the reversible transition, the minimum of the intensity and the desorption peak further shift to lower temperatures and both the minimum and the peak show a significant broadening. Also the shoulder on the desorption peak shifts to lower temperatures and broadens. For this film, the SR intensity, after the transition at higher temperature, is higher than the other three films and also the slope between 350 K and 430 K is similar to the slope of curve E which is recorded from a bare gold surface. All these results are consistent with a reversible melting transition that was also observed for thiol SAMs by means of scanning tunneling microscopy, helium diffraction and X-ray diffraction before in the range of 320 K-350 K.[15,17,46]

The changes which follow upon annealing to 400 K can be explained by a partial desorption of molecules/moieties from the film. The desorbed species leave behind more space for the remaining molecules in the film and this increased freedom allows the film to melt at lower temperatures. Moreover if significant parts of the film are desorbed, the uncovered bare substrate left behind contribute to the scattering intensity with a substantial increase of the intensity. Molecules at the borders of domains are less bonded and can desorb at lower temperature. Hence a defective film

starts to desorb at lower temperatures and the transition is also broader with respect to a more ordered film.

Since 265 K is in the phase transition temperature interval, the ML film grown at this temperature is a transition structure from the LT phase to HT phase. The phase transition temperature (250 K - 275 K) also overlaps with the temperature range for which the SR recovery due to completion of ML in the deposition curves is not pronounced (265 K – 300 K), shown in part I. This is not surprising since during the phase transition the ML may be going through a disordered state, which will limit the SR intensity recovery level due to completion of ML. The evolution of the diffraction patterns crossing the transition is analyzed below.

Diffraction patterns of the MLs recorded after the thermal treatment steps detailed above are given in Figure 6. The ML film grown at 200 K is not ordered and show very broad diffraction peaks. As discussed before, the film irreversibly changes into a different structure above 275 K annealing temperature. Moreover, all the diffraction patterns recorded after annealing to temperatures higher than 300 K present similar overall structure. However with increasing annealing temperature, SR and diffraction peak intensities increase. After a short 400 K annealing, diffraction peak positions shift to lower $\Delta K_{//}$ values along the <1-10> direction, which indicate that the unit cell expanded. This shift is evident for the peaks indicated with arrows in between -1.7 $Å^{-1}$ and -0.9 $Å^{-1}$. Along the <11-2> direction however there is no change in the positions of $\sqrt{3}$ peaks.

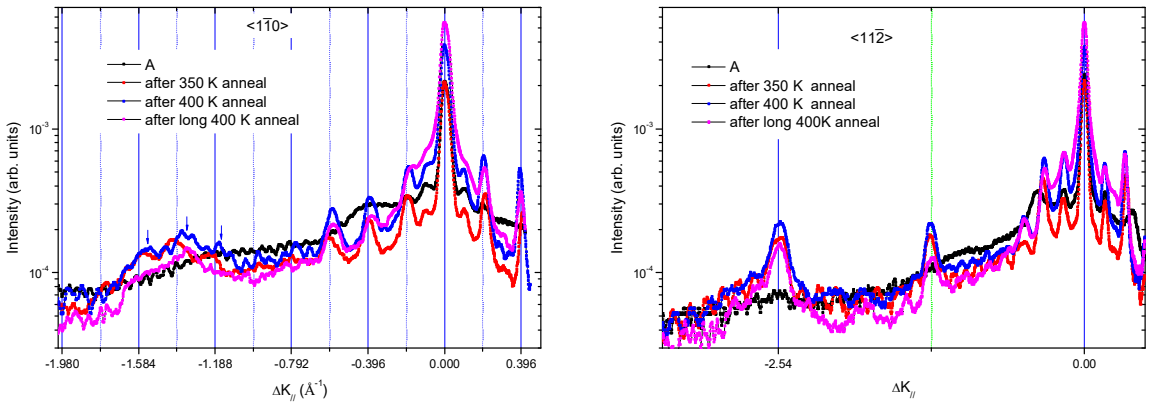

Figure 6. Diffraction scans of HDD ML films grown at 200 K substrate temperature after different thermal treatment steps measured along the main azimuthal directions of Au(111). Vertical lines indicate the expected peak positions for (11x$\sqrt{3}$) striped phase unit cell of DT.

In addition after 400 K annealing the noise in the diffraction signal considerably increased and this is due to thiol contamination in the chamber caused by the desorption from the sample and the crystal holder which causes condensation of thiols also on the cold detector as observed by authors in previous investigation of thiols. Expansion of the unit cell of thiol SAMs was also observed for the lying down phases of decanethiol by Sibener and co-workers after 400 K annealing.[50] One of the possible explanations they proposed was a partial desorption leading to a relaxation of the striped phase due to the surface area freed by the desorbing molecules. A similar process is taking place in our case as evidenced by the following observations: With longer annealing at 400 K, SR intensity increases considerably tending to the bare gold value while diffraction peak intensities decrease without any further shift in their positions. Hence partial desorption is taking place at 400 K causing some part of the gold surface to be freed and reducing the average domain size of the organic film and its coverage. This can also explain the observed shift in the melting transition temperature. In fact Porier and co-workers, investigating the phase diagrams of thiol SAMs in

detail, [17,51] predicted that the temperature of the transition between lying down phase and the lying down liquid phase should shift to lower temperatures with decreasing coverage.

DISCUSSION

Here we will comment on the relation between the thermal behavior and structural properties of HDD films and those of pure decanethiol (DT) and mercaptoundecanol (MUD) SAMs that we had studied in the past with the same techniques/procedures. [15,52] Structural and thermal properties of HDD SAMs studied here are summarized in Tables 1 and 2 along with the properties of DT and MUD SAMs that were reported before. The desorption energies listed in Table 2 were determined by performing a Redhead analysis after correcting the annealing curves shown in Figures 6.b for Debye-Waller effect and detector sensitivity.

Table 1. Unit Cell Parameters for the Striped Phases of DT, MUD, and HDD SAMs.

Molecule	Length[a] (Å)	P	Lattice constant (Å)	Reciprocal lattice constant ($Å^{-1}$)
DT[b]	13.6	x 11	31.7	0.198
MUD[c]	15.8	x 11.8[d]	34.0	0.184
HDD	31.0	x 11	31.7	0.198
Expanded HDD	31.0	x 11.3	32.6	0.193

[a] Reported values are the theoretical distances, calculated at AM1 level, from the center of sulfur atom to the center of furthest hydrogen atom in thiols and from the center of H atom at one end to the center of the H atom at the other end in the disulfides [b] Reported values for DT are taken from ref. 15 [c] Reported values for MUD are taken from ref 44 [d] In ref. 45 this value was reported to be 12.

Table 2. Melting Temperature and the Desorption Energies for the Striped Phases of DT, MUD and HDD SAMs.

Molecule	Melting Temperature[a] (K)	Desorption Energy (kJ/mol)		
		ML		
		Desorption 1 (kJ/mol)	Desorption 2 (kJ/mol)	Desorption 3 (kJ/mol)
DT[b]	355	125	140	
MUD[c]	400	118	136, 141	150
HDD	350	128	140	146

[a] Since the melting transitions are not sharp (see Figure 6) here approximate temperatures where melting starts are given. [b] Reported values for DT are taken from ref 15 [c] Reported values for MUD are taken from ref 44

In Figure 7 diffraction patterns and thermal behavior of HDD, MUD and DT SAMs are shown for comparison. From the diffraction data given in Figure 6 it is clear that periodicity of HDD SAMs at 300 K and 350 K (during growth or annealing), i.e. in the HT phase, is very similar to that of DT SAM. For instance when (-1.8 $Å^{-1}$) – (-1.0 $Å^{-1}$) region of the diffraction scan in Figure 6 is examined it can clearly be seen that for DT and HDD SAMs there are three overlapping peaks whereas for MUD SAMs there are only two peaks. In fact peak positions for HDD film annealed to 350 K matches well with the expected peak positions for (11x√3) striped phase unit cell of DT. If one assumes HDD SAM is made up of separate decanethiolate (-S-$(CH_2)_9$-CH_3, DTT) and hydroxyundecylthiolate (-S-$(CH_2)_{11}$-OH, MUDT) domains than the overall diffraction pattern can be obtained as an incoherent sum of the diffraction patterns of the separate domains. With this assumption, to determine the contribution of each thiolate domain to the HDD diffraction pattern, we performed a simulation by linearly combining the DT and MUD diffraction patterns shown in Figure 7. Such an analysis yields that the contribution from MUDT cannot be more than 10%. Hence, from the diffraction pattern of HDD we can conclude that there is a phase separation of

DTT and MUDT species where MUDT groups do not form ordered domains or the size of these domains are too small to yield measurable diffraction signal.

At higher temperatures however the diffraction peaks shift to smaller $\Delta K_{//}$ values indicating an expansion of the film. After annealing to 400 K the film expands by about 3% and the observed peak positions indicate the formation of a (11.3 x √3) unit cell. This expansion amount is very close to the expansion observed by Sibener and co-workers for DT films annealed to 400 K.[50]

Finally, the thermal behavior of HDD SAMs is similar to that of DT SAMs, with both going through a melting transition at about 350 K and having very close desorption temperatures. However in case of the HDD MLs there are three desorption states with energies of 128 kJ/mol, 140 kJ/mol and 146 kJ/mol whereas for DT only two were reported before. Most probably in the HDD MLs the low energy (118 kJ/mol) desorption state of MUD is suppressed and the high energy (136 kJ/mol, 141kJ/mol) MUD states are convoluted with those of DT, resulting in the observed thermal behavior of HDD MLs.

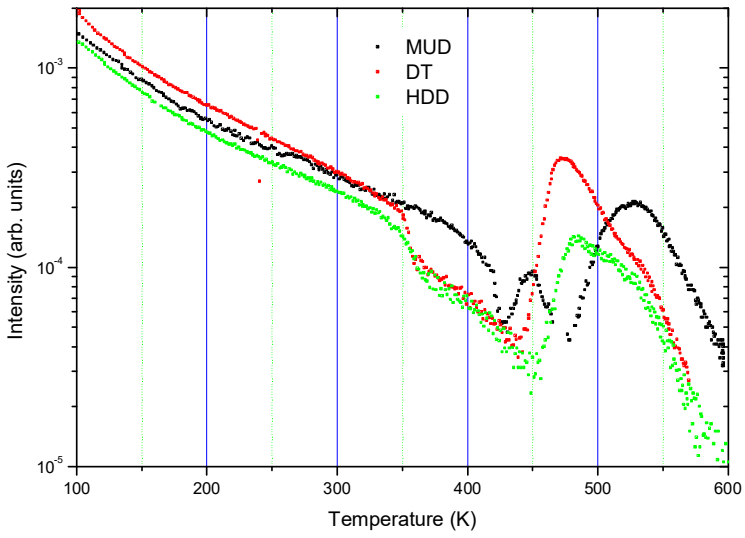

a)

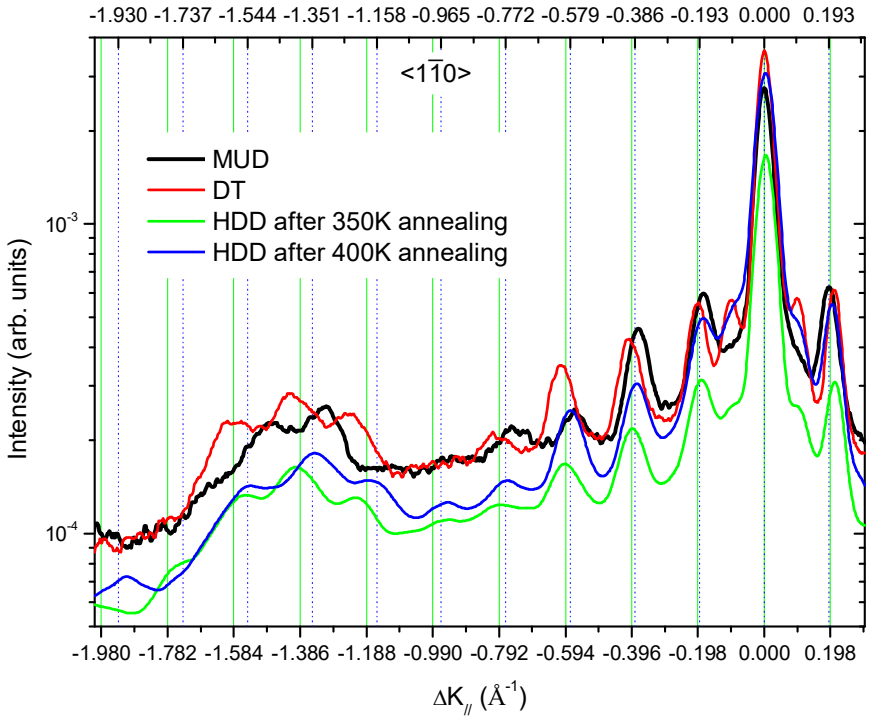

b)

Figure 7. a) Annealing curves for MLs of MUD, DT and HDD. b) Diffraction scans of MLs of MUD, DT and HDD. Solid grid lines indicate the expected peak positions for (11 x √3) unit cell. Dotted grid lines indicate the peak positions of the expanded film and correspond to a (11.3 x √3) unit cell. HDD diffraction scans are smoothed by adjacent point averaging for clarity

Summarizing, the results give a consistent picture of the deposition and thermal behavior of HDD on Au(111): for temperatures greater than 275 K the HT phase is formed while below 250 K a structurally different LT phase is adsorbed and this irreversibly converts into the HT phase around 275 K. The structure of the HT phase is very similar to DT SAMs and the MUDT fragments form a film with small domains that do not contribute appreciably to diffraction. On the other hand, there are open questions such as the structure of the LT phase, the size of the MUDT domains and their distribution that require further studies also with techniques different from He diffraction such as scanning probe and X-ray photoelectron spectroscopy techniques, possibly coupled with

SMBD to reproduce the present conditions, to better define the details of this process and this will be the aim of future investigations.

CONCLUSION

Long chain disulfide SAMs on Au(111) surface were for the first time grown in vacuum by means of SMBD. This technique allows a precise dosing of disulfides to study also the adsorption at very low coverage. The film has been characterized by He diffraction and measurements have been performed for different substrate temperatures also in real-time during the growth of the film. Diffraction patterns from films grown in different conditions and after thermal treatments have been acquired on the lying down phase and compared with the diffraction pattern of films of the two moieties which form the disulfide. The film desorption has been also studied to evaluate desorption energies.

The results show that the film undergoes two transitions. The transition around 275 K is irreversible and all the diffraction data point out a phase separation while the transition around 350 K is reversible and can be related to the melting of the film. Desorption from several different chemisorbed states were observed with energies in the same range as observed for DT and MUD SAMs.

AUTHOR INFORMATION

Corresponding Author

*E-mail: danisman@metu.edu.tr

ACKNOWLEDGMENT

This work was supported by The Scientific and Technological Research Council of Turkey, TÜBİTAK, Grant No. 209T084.

REFERENCES

[1] R. K. Smith, P. A. Lewis, and P. S. Weiss, Progress in Surface Science **75,** 1 (2004).
[2] J. C. Love, L. A. Estroff, J. K. Kriebel, R. G. Nuzzo, and G. M. Whitesides, Chemical Reviews **105,** 1103 (2005).
[3] C. Vericat, M. E. Vela, G. Benitez, P. Carro, and R. C. Salvarezza, Chemical Society Reviews **39,** 1805 (2010).
[4] F. Schreiber, Progress in Surface Science **65,** 151 (2000).
[5] Z. Matharu, A. J. Bandodkar, V. Gupta, and B. D. Malhotra, Chemical Society Reviews **41,** 1363 (2012).
[6] P. Thevenot, W. J. Hu, and L. P. Tang, Current Topics in Medicinal Chemistry **8,** 270 (2008).
[7] N. J. Tao, Nature Nanotechnology **1,** 173 (2006).
[8] M. F. Danisman, L. Casalis, G. Bracco, and G. Scoles, Journal of Physical Chemistry B **106,** 11771 (2002).
[9] N. Nishi, D. Hobara, M. Yamamoto, and T. Kakiuchi, Journal of Chemical Physics **118,** 1904 (2003).
[10] Q. Guo, X. Sun, and R. E. Palmer, Physical Review B **71** (2005).
[11] R. Mazzarello, A. Cossaro, A. Verdini, R. Rousseau, L. Casalis, M. F. Danisman, L. Floreano, S. Scandolo, A. Morgante, and G. Scoles, Physical Review Letters **98** (2007).
[12] A. Cossaro, R. Mazzarello, R. Rousseau, L. Casalis, A. Verdini, A. Kohlmeyer, L. Floreano, S. Scandolo, A. Morgante, M. L. Klein, and G. Scoles, Science **321,** 943 (2008).
[13] F. S. Li, L. Tang, W. C. Zhou, and Q. M. Guo, Journal of the American Chemical Society **132,** 13059 (2010).
[14] L. P. M. De Leo, E. de la Llave, D. Scherlis, and F. J. Williams, Journal of Chemical Physics **138** (2013).
[15] E. Albayrak, S. Duman, G. Bracco, and M. F. Danisman, Applied Surface Science **268,** 98 (2013).
[16] Y. L. Qian, G. H. Yang, J. J. Yu, T. A. Jung, and G. Y. Liu, Langmuir **19,** 6056 (2003).
[17] G. E. Poirier, W. P. Fitts, and J. M. White, Langmuir **17,** 1176 (2001).
[18] P. Maksymovych, O. Voznyy, D. B. Dougherty, D. C. Sorescu, and J. T. Yates, Progress in Surface Science **85,** 206 (2010).
[19] D. P. Woodruff, Physical Chemistry Chemical Physics **10,** 7211 (2008).
[20] F. Schreiber, A. Eberhardt, T. Y. B. Leung, P. Schwartz, S. M. Wetterer, D. J. Lavrich, L. Berman, P. Fenter, P. Eisenberger, and G. Scoles, Physical Review B **57,** 12476 (1998).
[21] N. Camillone, T. Y. B. Leung, P. Schwartz, P. Eisenberger, and G. Scoles, Langmuir **12,** 2737 (1996).
[22] F. Balzer, R. Gerlach, G. Polanski, and H. G. Rubahn, Chemical Physics Letters **274,** 145 (1997).
[23] L. H. Dubois, B. R. Zegarski, and R. G. Nuzzo, Journal of Chemical Physics **98,** 678 (1993).
[24] P. Schwartz, F. Schreiber, P. Eisenberger, and G. Scoles, Surface Science **423,** 208 (1999).

[25] G. Bracco and G. Scoles, Journal of Chemical Physics **119,** 6277 (2003).
[26] J. E. Raynor, J. R. Capadona, D. M. Collard, T. A. Petrie, and A. J. Garcia, Biointerphases **4,** FA3 (2009).
[27] J. P. Folkers, P. E. Laibinis, G. M. Whitesides, and J. Deutch, Journal of Physical Chemistry **98,** 563 (1994).
[28] S. J. Stranick, A. N. Parikh, Y. T. Tao, D. L. Allara, and P. S. Weiss, Journal of Physical Chemistry **98,** 7636 (1994).
[29] S. V. Atre, B. Liedberg, and D. L. Allara, Langmuir **11,** 3882 (1995).
[30] S. J. Stranick, S. V. Atre, A. N. Parikh, M. C. Wood, D. L. Allara, N. Winograd, and P. S. Weiss, Nanotechnology **7,** 438 (1996).
[31] K. Tamada, M. Hara, H. Sasabe, and W. Knoll, Langmuir **13,** 1558 (1997).
[32] D. Hobara, T. Sasaki, S. Imabayashi, and T. Kakiuchi, Langmuir **15,** 5073 (1999).
[33] S. F. Chen, L. Y. Li, C. L. Boozer, and S. Y. Jiang, Langmuir **16,** 9287 (2000).
[34] F. Tantakitti, J. Burk-Rafel, F. Cheng, R. Egnatchik, T. Owen, M. Hoffman, D. N. Weiss, and D. M. Ratner, Langmuir **28,** 6950 (2012).
[35] B. P. Pichon, M. Pauly, P. Marie, C. Leuvrey, and S. Begin-Colin, Langmuir **27,** 6235 (2011).
[36] N. J. Brewer and G. J. Leggett, Langmuir **20,** 4109 (2004).
[37] K. Heister, D. L. Allara, K. Bahnck, S. Frey, M. Zharnikov, and M. Grunze, Langmuir **15,** 5440 (1999).
[38] J. Z. Gao, F. S. Li, and Q. M. Guo, Langmuir **29,** 11082 (2013).
[39] M. W. Tsao, J. F. Rabolt, H. Schonherr, and D. G. Castner, Langmuir **16,** 1734 (2000).
[40] T. Takami, E. Delamarche, B. Michel, C. Gerber, H. Wolf, and H. Ringsdorf, Langmuir **11,** 3876 (1995).
[41] S. F. Chen, L. Y. Li, C. L. Boozer, and S. Y. Jiang, Journal of Physical Chemistry B **105,** 2975 (2001).
[42] S. M. Flores, A. Shaporenko, C. Vavilala, H. J. Butt, M. Schmittel, M. Zharnikov, and R. Berger, Surface Science **600,** 2847 (2006).
[43] J. Noh and M. Hara, Langmuir **16,** 2045 (2000).
[44] E. Albayrak and M. F. Danisman, Journal of Physical Chemistry C **117,** 9801 (2013).
[45] Y. C. Yang, T. Y. Chang, and Y. L. Lee, Journal of Physical Chemistry C **111,** 4014 (2007).
[46] G. H. Yang and G. Y. Liu, Journal of Physical Chemistry B **107,** 8746 (2003).
[47] M. F. Danisman and B. Ozkan, Review of Scientific Instruments **82** (2011).
[48] D. Miller, in *Atomic and Molecular Beam Methods*; *Vol. 1*, edited by G. Scoles (Oxford University Press, New York, 1992), p. 14.
[49] P. A. Redhead and J. P. Hobson, Vacuum **15,** 25 (1965).
[50] S. B. Darling, A. W. Rosenbaum, Y. Wang, and S. J. Sibener, Langmuir **18,** 7462 (2002).
[51] G. E. Poirier, Langmuir **15,** 1167 (1999).
[52] E. Albayrak and M. F. Danışman, The Journal of Physical Chemistry C (2013).